ARTICLES SCIENCE CHINA Materials

mater.scichina.com link.springer.com

Published online 28 December 2015 | doi: 10.1007/s40843-015-0110-x
Sci China Mater 2015, 58: 944–952

Microwave-assisted synthesis of layer-by-layer ultra-large and thin NiAl-LDH/RGO nanocomposites and their excellent performance as electrodes

Zhuo Wang[1,2], Wei Jia[1], Menglei Jiang[1], Chen Chen[1*] and Yadong Li[1]

In this work, ultra-large sheet NiAl-layered double hydroxide (LDH)/reduced graphene oxide (RGO) nanocomposites were facilely synthesized via *in situ* growth of NiAl-LDH on a graphene surface without any surfactant or template. It was found that with a microwave-assisted method, NiAl-LDH nanosheets grew evenly on the surface of graphene. With this method, the formation of NiAl-LDH and reduction of graphene oxide were achieved in one step. The unique structure endows the electrode materials with a higher specific surface area, which is favorable for enhancing the capacity performance. The morphology and microstructure of the as-prepared composites were characterized by X-ray diffraction, Brunauer-Emmett-Teller surface area measurement, and transmission electron microscopy . The specific surface area and pore volume of the RGO/LDH composite are 108.3 $m^2 g^{-1}$ and 0.74 $cm^3 g^{-1}$, respectively, which are much larger than those of pure LDHs (19.8 $m^2 g^{-1}$ and 0.065 $cm^3 g^{-1}$, respectively). The capacitive properties of the synthesized electrodes were studied using cyclic voltammetry and electrochemical impedance spectroscopy in a three-electrode experimental setup. The specific capacitance of RGO/LDHs was calculated to be 1055 F g^{-1} at 1 A g^{-1}. It could be anticipated that the synthesized electrodes will find promising applications as novel electrode materials in supercapacitors and other devices because of their outstanding characteristics of controllable capacitance and facile synthesis.

INTRODUCTION

In recent years, the energy crisis has become increasingly severe because of the over-consumption of energy. Researchers have dedicated themselves to energy storage and conversion from environmentally friendly resources [1,2]. Electrochemical capacitors, also called supercapacitors, are promising energy storage devices that can be used as a backup power source in portable electronic devices, pacemakers, and hybrid electrical vehicles, and have gained rapidly increasing attention for their unique properties, such as high power density, long cycle life, and small size [3–7]. Depending on the charge storage mechanism, supercapacitors can be divided into two basic classes: electric double layer capacitance (EDLC) and pseudocapacitance [8]. The former generates capacitance from charge separation at the electrode/electrolyte interface [9,10], while the latter generates capacitance from the fast Faradaic reactions in electrode materials [11]. The performance of a supercapacitor is closely related to the physical and chemical features of the electrode materials. Usually, electrode materials containing carbon-based materials are regarded as typical EDLC supercapacitors, where the capacitance depends on the specific surface area, porous structure, and conductivity of active materials. Carbon-based materials possess long cycle lives and good mechanical properties. Pseudocapacitive active species include metal oxides (MnO_2, Co_3O_4, RuO_2, Fe_2O_3, AB_2O_4), conducting polymers (polyaniline, polypyrrole, and polythiophene), and hydroxides [11–21]. These materials can deliver relatively high capacitance but are limited by poor stability because of structural degradation of the electrode during the redox process [22,23]. Thus, the capacitance can be enhanced by incorporating carbon materials with pseudocapacitive materials.

Layered double hydroxides (LDHs), a kind of anionic clay, have attracted extensive attention owing to their intriguing properties, such as large surface area, positively charged surface, and compositional flexibility [24,25]. LDHs are usually expressed as the following formula: $[M^{2+}_{1-x}M_x^{3+}(OH)_2]^{x+}[A^{n-}]_{x/n}{\cdot}mH_2O$, in which M^{2+} and M^{3+} are divalent and trivalent metal cations, respectively, and A^{n-} is an interlayer anion. The tunable composition and their anion exchange ability allow LDHs to be used as a variety of multifunctional materials, such as catalysts, absorbents, photoactive materials, and electroactive materials [26–29]. Thus far, LDH nanomaterials used as electrodes have been widely studied. Niu *et al.* [30] reported

[1] Department of Chemistry and Collaborative Innovation Center for Nanomaterial Science and Engineering, Tsinghua University, Beijing 100084, China
[2] Institute of Electrical Engineering, Chinese Academy of Sciences, Beijing 100190, China
[*] Corresponding author (email: cchen@mail.tsinghua.edu.cn)

that NiAl-LDH grown on well-activated graphene sheets provides a maximum specific capacitance of 1730.2 F g^{-1} at a current density of 0.1 A g^{-1}. Li *et al.* [31] developed a facile method to synthesize a NiAl-LDH/graphene hybrid with enhanced electrochemical properties for detection of dopamine. Cheng *et al.* [32] synthesized self-supporting electrodes based on cobalt-nickel hydroxide using accumulative approaches. Yu *et al.* [33] reported nanohybrids of NiCoAl-LDH and carbon as pseudocapacitors.

Graphene with a one-atom-thick two-dimensional (2D) structure has been investigated intensively for its unique characteristics, such as chemical stability, high electrical conductivity, and large surface area [34]. Because of these intriguing characteristics, such new materials have a wide range of potential applications and have attracted great interest in the development of graphene composites [35,36]. The effective surface area of graphene materials is closely related to the layers; that is, materials containing fewer layers with agglomeration should be expected to exhibit higher effective surface areas. Thus, numerous methods have been used to enlarge the specific surface area of pristine graphene.

Ultra-thin 2D nanomaterials represent a very interesting target with great promising applications in next-generation batteries and supercapacitors [37]. However, compared with other ultra-thin and large 2D nanosheets, the synthesis of ultra-thin and large 2D nanosheet LDHs grown on reduced graphene oxide (RGO) seems difficult. To the best of our knowledge, only Xu *et al.* [38] reported an ultra-large and thin sandwich-type three-dimensional (3D) LDH nanosheet array/graphene composite using AlOOH as a template. Thus, facile synthesis of graphene/LDH nanosheets with ultra-thin films should be developed and explored for their potential as supercapacitors.

In the present work, large RGO/LDH sheets were facilely synthesized; the formation of LDHs and reduction of graphene oxide (GO) were achieved simultaneously in one step. The formation of LDHs on RGO was discussed in detail. Electrochemical performances of the materials were investigated by cyclic voltammetry (CV), galvanostatic charge/discharge cycling, and electrochemical impedance spectroscopy (EIS) studies. The supercapacitor materials, which were expected to give high performances, were synthesized and studied.

EXPERIMENTAL SECTION

Preparation of graphene oxide and graphene/LDH nanosheets

GO was prepared from natural graphite powder through a modified Hummers' method [39]. Graphene/LDH nanosheets were prepared as follows: a certain amount of GO was dispersed in H_2O, stirred, and ultrasonicated for 2 h to form a homogeneous aqueous dispersion (solution A). Then, 0.29 g $Ni(NO_3)_2$, 0.19 g $Al(NO_3)_3$, and 0.36 g urea were added to a mixture of H_2O and ethylene glycol followed by stirring at room temperature (solution B). Then, solution B was poured into solution A, and heated at 180°C using a microwave-assisted method for several minutes for crystallization, until the brown reaction solution became black, indicating the reduction of GO to RGO. LDHs were synthesized via similar methods without the addition of GO. The products were washed with deionized water several times and dried at 50°C for 24 h. The samples were denoted as RGO/LDHs and LDHs, respectively.

Material characterization

The X-ray diffraction (XRD) patterns of the samples were collected on a Rigaku D/max-2400 diffractometer operated at 40 kV and 200 mA with Cu Kα radiation (λ = 1.5418 Å). The morphologies were analyzed using transmission electron microscopy (TEM, Hitachi H-800) and scanning electron microscopy (SEM, Hitachi S-3000N) techniques. High-resolution TEM (HRTEM) images were recorded using an FEI Tecnai G2 F20 S-Twin high-resolution transmission electron microscope working at 200 kV and an FEI Titan 80–300 transmission electron microscope equipped with a spherical aberration (Cs) corrector for the objective lens working at 300 kV. Adsorption and desorption isotherms of nitrogen were measured with a NOVA 1200 gas sorption analyzer at liquid nitrogen temperature (−196°C). Before the measurements, the samples were degassed under vacuum at 120°C for 8 h. The total pore volume was estimated from the amount of nitrogen adsorbed at a relative pressure of 0.99. The Brunauer-Emmett-Teller (BET) method was utilized to calculate the specific surface area using adsorption data acquired at a relative pressure (P/P_0) range of 0.05–0.25. The pore size distribution curves were calculated from the analysis of the desorption branch of the isotherm based on the Barrett-Joyner-Halenda (BJH) algorithm. The micropore volume and micropore surface area were estimated using a t-plot method.

Electrochemical measurements

All of the electrochemical measurements were carried out in a conventional three-electrode system in a 6 mol L^{-1} KOH aqueous electrolyte at room temperature. The as-synthesized electrode materials, a platinum wire electrode, and a silver chloride electrode (Ag/AgCl) were used as the working electrode, counter electrode, and reference elec-

trode, respectively. The working electrode was prepared by mixing the sample (75 wt.%) as the active material with poly(tetrafluoroethene) (PTFE, 10 wt.%) and carbon black (15 wt.%) in ethanol to produce a homogeneous paste. Then, the resulting mixture was coated onto the Ni foam substrate. The foam was dried at 80°C in air for 12 h to remove the solvent. The electrochemical performances of the as-prepared material electrodes were tested using a CV method, galvanostatic charge/discharge, and EIS on an electrochemical workstation (CHI 660D, Shanghai CH Instrument Company, China). CV tests were done between 0 and 0.5 V (*vs*. Ag/AgCl) at scan rates of 10, 20, 30, 40, 50, and 100 mV s^{-1}. Galvanostatic charge/discharge curves were measured in the potential range of 0–0.4 V at different current densities, and the EIS measurements were carried out in the frequency range from 100 kHz to 0.5 Hz at open circuit potential with an alternating current perturbation of 5 mV.

RESULTS AND DISCUSSION

The formation of RGO/LDHs can be explained as follows (Scheme 1). Metal cations were initially adsorbed on the GO surface, and then urea decomposition via a microwave-assisted heating method, reduction of GO, and crystallization of LDH sheets proceeded in one step. Powder XRD patterns of LDHs and RGO/LDHs nanocomposites are given in Fig 1. It can be clearly seen that the characteristic reflections of (003), (006), (012), and (110) corresponding to 2D hydrotalcite-like materials are present in each sample [31]. The *d*-spacing between the basal planes of the double hydroxide was 9.1692 Å, while that of RGO/LDHs nanomaterials was 10.130 Å, revealing the peeling-off of graphene. The XRD spectrum of RGO/LDHs nanocomposites that are similar to LDHs reveals the formation of LDHs on the surface of RGO. However, no diffraction peak corresponding to RGO stacks (at ~25°) was observed, indicating that most of the graphene sheets were covered by hydroxides, and therefore the layer-to-layer interaction between adjacent graphene sheets, as in a pure graphene film, is significantly reduced in the composite [32]. The diffraction peak at ~10° corresponding to GO (Fig. 1) completely disappears after the reaction, demonstrating that GO can

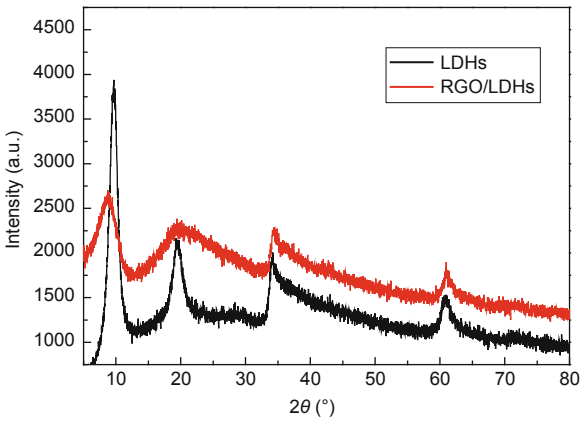

Figure 1 XRD patterns of LDHs (a) and RGO/LDHs (b) samples.

be reduced in the presence of urea using the microwave method, which has been confirmed in the literature [40].

In order to further investigate the morphologies of LDHs and RGO/LDHs, the nanohybrids were characterized by SEM, TEM, and HRTEM measurements, as shown in Figs 2 and 3. The SEM image of NiAl-LDH (Fig. 2a) indicates that the nanomaterial consists of a large number of sheets, which aggregated randomly to form a flower-like structure, while the SEM image of RGO/LDHs shows that, unlike pure LDHs, the composites are composed of ultra-large sheet-like structures, and LDH nanosheets are grown evenly on the surface of RGO (Fig. 2b). The representative TEM images of LDHs and RGO/LDHs, shown in Figs 3a and b, further indicate that pure LDHs possess a flower-like structure with sheets stacked randomly, while RGO/LDHs in the presence of GO interconnected with each other, forming a homogeneous nanostructure. In order to further distinguish the distribution of RGO and NiAl-LDHs, these nanomaterials were investigated using high-angle annular dark-field scanning transmission electron microscopy (HAADF-STEM). As can be seen from the energy dispersive spectroscopy (EDS) mapping results (Fig. 3), RGO and LDHs are integrated evenly.

As we know, textural properties, including the surface area and pore size distribution, play important roles in supercapacitor performance. The porous structure of LDHs

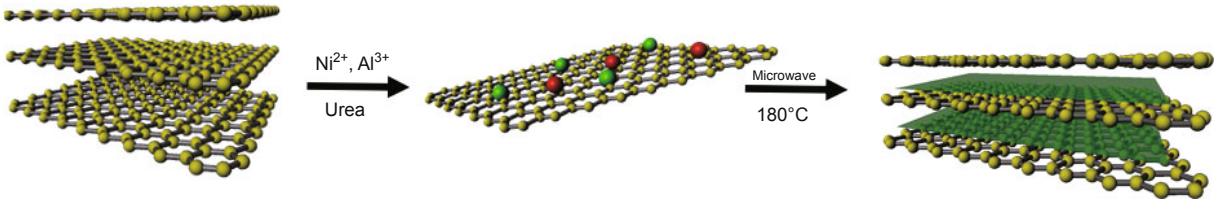

Scheme 1 The formation of ultra large and thin NiAl-LDH/RGO nanocomposites.

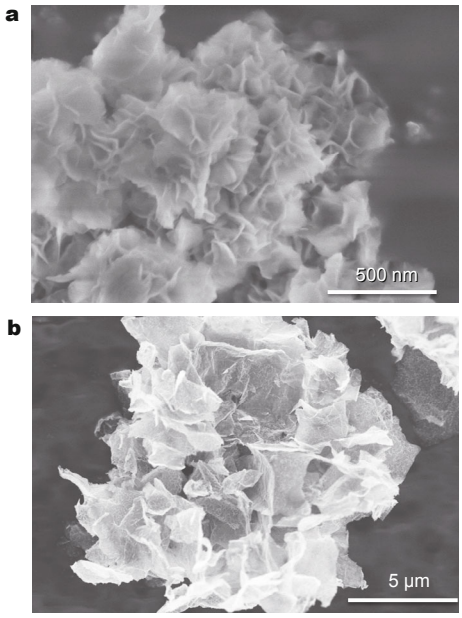

Figure 2 SEM images of LDHs (a) and RGO/LDHs (b) samples.

and RGO/LDHs were characterized by nitrogen adsorption. These composites possess well-developed mesoporosity, as reflected by their N_2 sorption isotherm and large N_2 uptake at low relative pressure. However, the pore size distributions are not uniform and are different from each other (Fig. 4). As can be seen, RGO/LDHs possesses higher specific surface area and wider range of pore size distribution. The specific surface area and pore volume of the RGO/LDHs composite are 108.3 $m^2 g^{-1}$ and 0.74 $cm^3 g^{-1}$, respectively, which are much larger than those of pure LDHs (19.8 $m^2 g^{-1}$ and 0.065 $cm^3 g^{-1}$, respectively). Thus, it is deduced that the *in situ* growth of LDHs on RGO is beneficial to the peeling of graphene sheets, which leads to the increase in the specific surface area. Further, from the pore size distribution of these two samples, RGO/LDHs show a wide range of pore size distribution, owing to the combination of RGO and LDHs. Moreover, samples with high specific surface areas and mesopores are favorable for improving both the main pseudocapacitance of metals and the EDLC of graphene because of the easily accessible na-

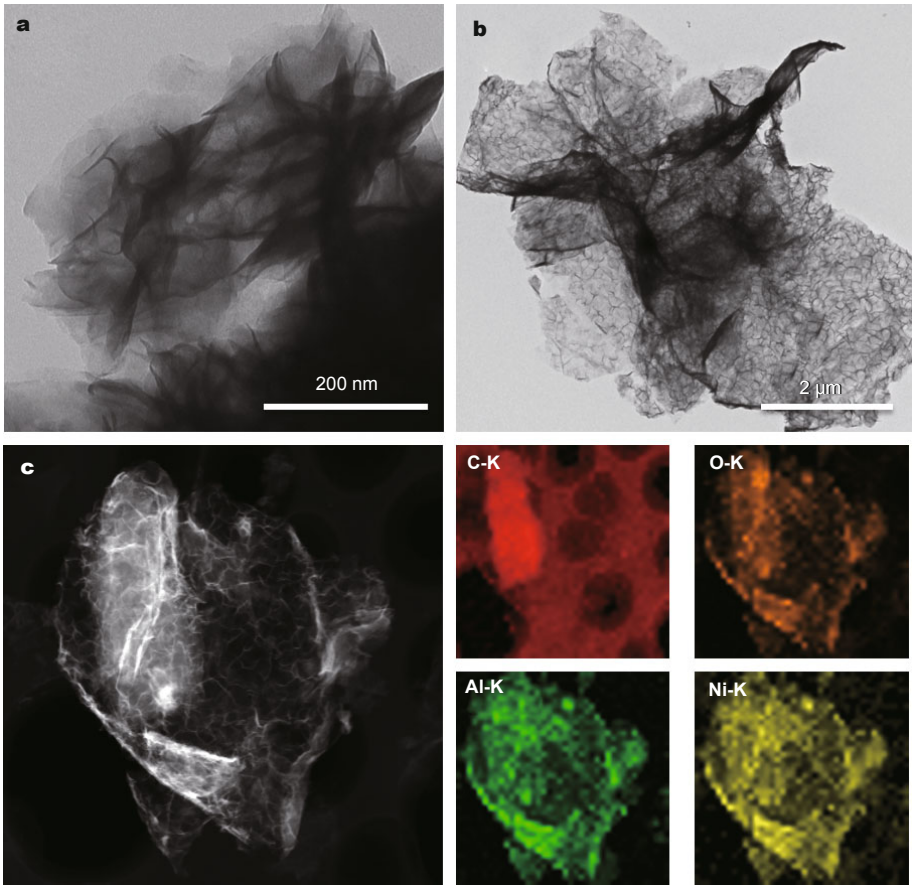

Figure 3 TEM images of LDHs (a) and RGO/LDHs (b) samples; (c) EDX mapping results of RGO/LDHs nanocomposites.

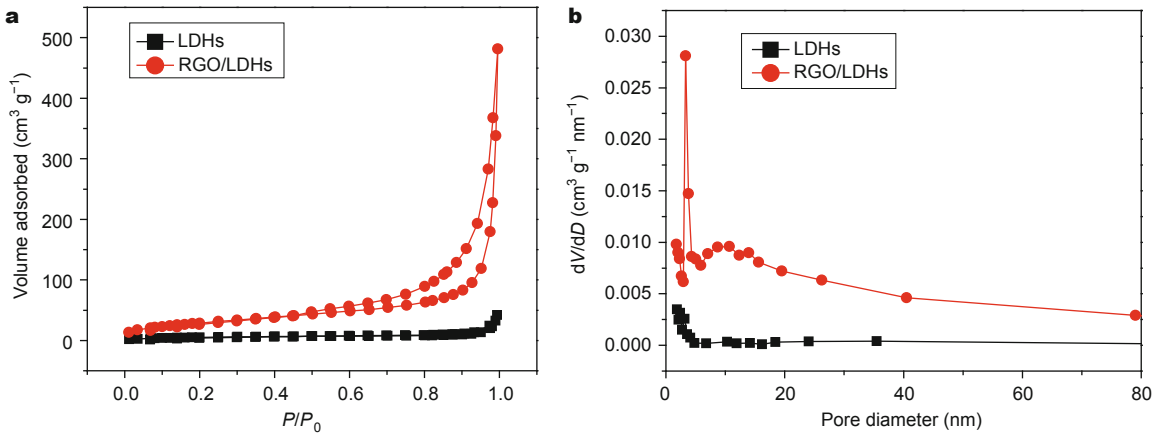

Figure 4 Nitrogen adsorption/desorption isotherms (a) and BJH pore size distributions (b) for LDHs and RGO/LDHs nanocomposites.

ture of the hydrated ions in the electrolyte to the exterior and interior pore surfaces [41,42].

The electrochemical behaviors of the obtained RGO/LDHs and LDHs nanocomposites were investigated by CV, charge/discharge cycling, and EIS measurements. Figs 5a and b show the CV curves of the LDHs and RGO/LDHs electrodes at scan rates of 10, 20, 30, 40, 50, and 100 mV s^{-1} in a 6 mol L^{-1} KOH electrolyte between 0 and 0.5 V, respectively. As can be seen, the electrodes deviated from the typical electrochemical double-layer capacitive behavior. They contain a pair of redox peaks corresponding to the redox of Ni^{2+}/Ni^{3+} with OH^- [43,44], and it is obvious that the reduction and oxidation peaks exhibit a small shift with the increasing scan rates, corresponding to higher reversibility. In addition, from Fig. 5c, it is obvious that the CV curves of RGO/LDHs show higher integrated areas than those of pure LDHs, which indicates excellent electrochemical performance of the RGO/LDHs electrode material. The high

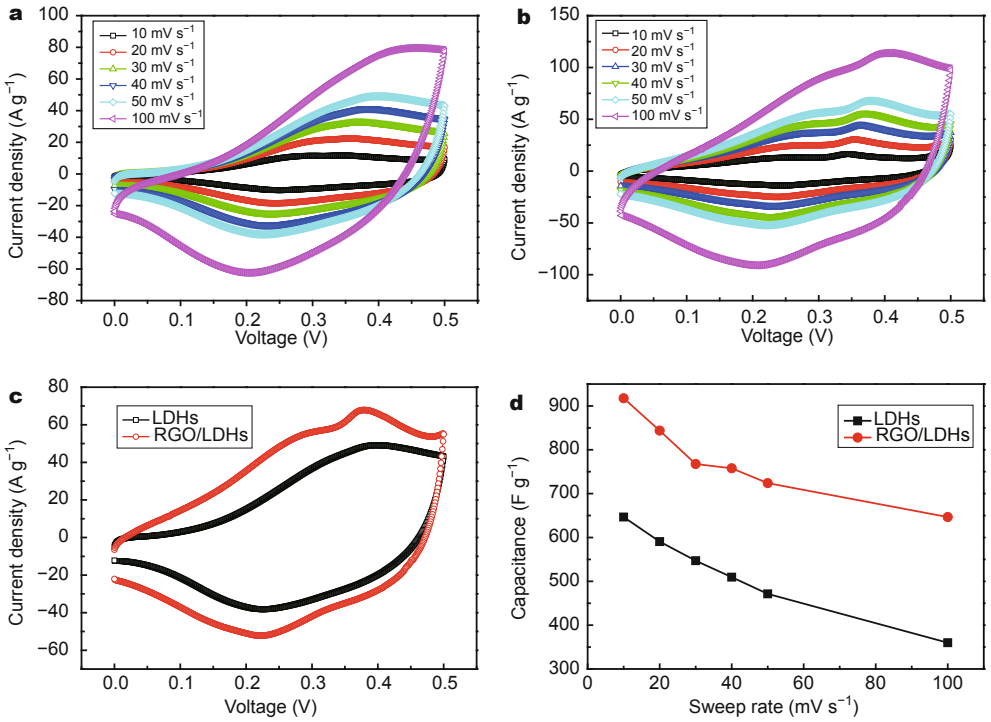

Figure 5 CV curves of LDHs (a) and RGO/LDHs (b) at different sweep rates; (c) comparison of the specific capacitances for the composite electrodes at the same sweep rate; (d) specific capacitances of LDHs and RGO/LDHs at different sweep rates.

electrochemical specific capacitance of RGO/LDHs can be ascribed to the appropriate experimental conditions that lead to the addition of LDHs and effectively prevent the agglomeration of RGO, thus leading to a higher active surface area for charge storage. The specific capacitances (C_s) were calculated from the CV curves according to the following equation:

$$C_s = \frac{\int I dV}{\upsilon m \Delta V},$$

where C_s is the specific capacitance based on the mass of electroactive materials (F g^{-1}), I is the response current (A), ΔV is the potential window (V), υ is the potential scan rate (mV s^{-1}), and m is the mass of the electroactive materials in the electrodes (g). The C_s values calculated from the CV curves of LDHs and RGO/LDHs at different sweep rates are given in Fig. 5d.

In order to further investigate the performance of the electrode materials, galvanostatic charge/discharge tests of LDHs and RGO/LDHs were conducted in 6 mol L^{-1} KOH with different current densities in a voltage range of 0–0.4 V, as shown in Fig. 6. The C_s of the electrodes can be calculated according to the following equation:

$$C_s = \frac{It}{(\Delta V)m},$$

where m (g) is the mass of the active material in the film electrode, I (A) is the discharge current, ΔV (V) is the potential window, t (s) is the discharge time, and C_s (F g^{-1}) is the specific capacitance. The RGO/LDHs nanocomposites show clearly higher specific capacitances and better rate capabilities than the pure LDHs, which is in accord with the trend of the C_s calculated from the CV curves. The specific capacitances of the composites were calculated to be 1055, 1024, 995, 973, and 939 F g^{-1}, at 1 to 5 A g^{-1}, respectively. The highest specific capacitance at current densities of 1 and 5 A g^{-1} gave a capacitive retention rate of 88.9%, exhibiting excellent rate capability. Furthermore, all of the values of RGO/LDHs calculated from the galvanostatic charge/discharge tests are higher than those of pure LDHs at all current densities. The increase might be caused by the combination of the EDLC of RGO and Faradaic pseudocapacitance of LDH layers.

Fig. 7 gives the Nyquist plots of RGO/LDHs and LDHs composite electrodes. In the high-frequency region, a semicircle due to charge transfer resistance on the electrode/electrolyte interface is observed. The region between the high- and low-frequency regions is called the Warburg region, and this is a combination of both resistive and capacitive behaviors characterized by diffusive resistance. The region in low frequency represents the swift ion diffusion in the electrolyte and the adsorption onto the electrode surface. The intersection of the semicircle and the

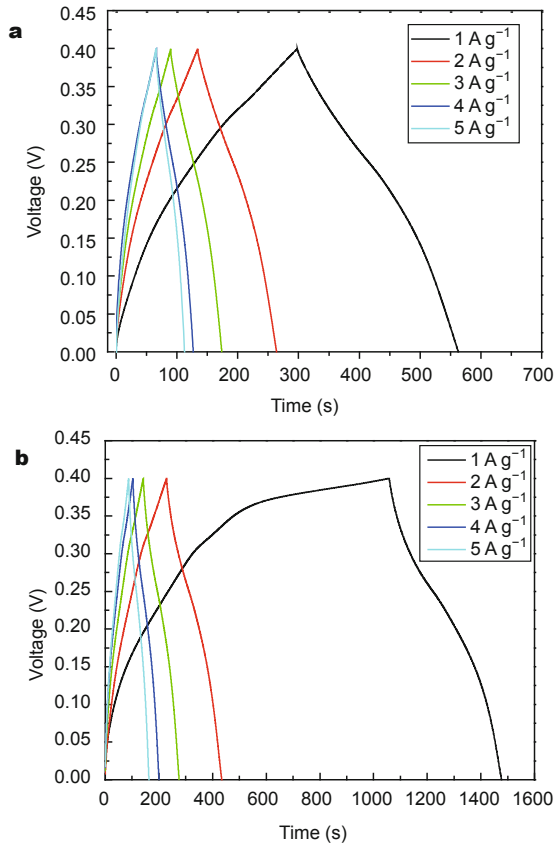

Figure 6 Galvanostatic charge-discharge curves of LDHs (a) and RGO/LDHs (b) at different current densities.

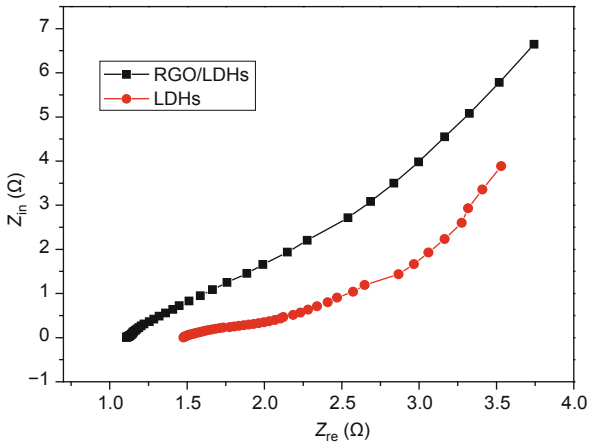

Figure 7 Comparison of the Nyquist plots of electrodes LDHs and RGO/LDHs.

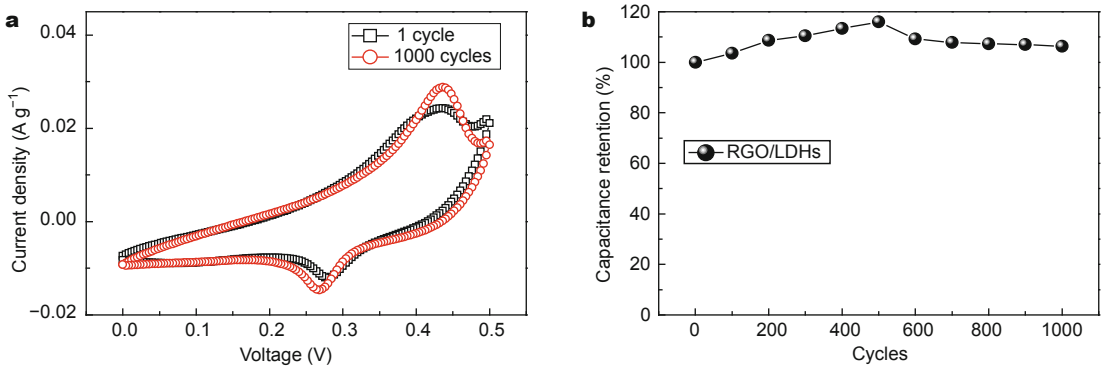

Figure 8 (a) Comparison of CV curves of RGO/LDHs for the first and last cycles. (b) Retention performance of RGO/LDHs at sweep rate of 50 mV s^{-1}.

real axis at high frequency represents the equivalent series resistance (R_s) of the electrode, while the diameter of the semicircle corresponds to the charge-transfer resistance (R_{ct}) of the electrodes and electrolyte interface [45]. Upon comparing the impedance plots of these electrodes, it is apparent that the values of R_s of LDHs are higher than those of RGO/LDHs. These results are partially caused by the low conductivity of the pure LDHs.

The electrochemical stability is an important parameter in the evaluation/assessment of the practical properties of a supercapacitor. Fig. 8 shows the cycling stability of the RGO/LDHs electrode materials determined using a CV technique at a sweep rate of 50 mV s^{-1} in the potential window of 0–0.5 V. It is apparent that the capacitance increases (116%) in the first 500 cycles, which is possibly because of the activation process. During this process, the unused electrochemically active Ni sites of the active material inside the nickel foam electrode are fully exposed to the electrolyte during the cycling process [46,47]. Then, after 500 cycles, the capacitance shows a slight decrease, even though the capacitance is higher than that in the first cycle, implying that the electrode is a promising electrode material.

CONCLUSIONS

In conclusion, a facile microwave-assisted method for synthesizing ultra-large RGO/LDHs composites was realized. The *in situ* growth of LDHs on RGO gives features including low thickness, larger specific surface area, and enhanced electrical conductivity. Their electrochemical properties as supercapacitors were discussed in detail; the unique structure of RGO/LDHs eventually leads to superior current capacitive behavior and good cycling performance compared with LDHs. It was found that good dispersion and proper particle size lead to good electrochemical properties. The as-synthesized nanocomposites utilized the benefits of metal hydroxides and the conductive EDLC nature of the RGO, implying good potential for application in supercapacitors as well as in other power source systems.

Received 4 December 2015; accepted 24 December 2015; published online 28 December 2015

1 Simon P, Gogotsi Y. Materials for electrochemical capacitors. Nat Mater, 2008, 7: 845–854
2 Gao Z, Wang J, Li ZS, *et al.* Graphene nanosheet/Ni^{2+}/Al^{3+} layered double-hydroxide composite as a novel electrode for a supercapacitor. Chem Mater, 2011, 23: 3509–3516
3 Wang L, Wang D, Dong XY, *et al.* Layered assembly of graphene oxide and Co–Al layered double hydroxide nanosheets as electrode materials for supercapacitors. Chem Comm, 2011, 47: 3556–3558
4 Xu YX, Huang XQ, Lin ZY, *et al.* One-step strategy to graphene/$Ni(OH)_2$ composite hydrogels as advanced three-dimensional supercapacitor electrode materials. Nano Res, 2013, 6: 65–76
5 Wei WF, Cui XW, Chen WX, *et al.* Manganese oxide-based materials as electrochemical supercapacitor electrodes. Chem Soc Rev, 2011, 40: 1697–1721
6 Wang HL, Liang YY, Mirfakhrai T, *et al.* Advanced asymmetrical supercapacitors based on graphene hybrid materials. Nano Res, 2011, 4: 729–736
7 Wang GP, Zhang L, Zhang JJ. A review of electrode materials for electrochemical supercapacitors. Chem Soc Rev, 2012, 41: 797–828
8 Conway BE. Transition from "supercapacitor" to "battery" behavior in electrochemical energy storage. J Electrochem Soc, 1991, 138: 1539–1548
9 Liu CF, Song HQ, Zhang CK, *et al.* Coherent Mn_3O_4-carbon nanocomposites with enhanced energy-storage capacitance. Nano Res, 2015, 8: 3372–3383
10 Frackowiak E. Carbon materials for supercapacitor application. Phys Chem Chem Phys, 2007, 9: 1774–1785
11 Chen PC, Chen HT, Qiu J, *et al.* Inkjet printing of single-walled carbon nanotube/RuO_2 nanowire supercapacitors on cloth fabrics and flexible substrates. Nano Res, 2010, 3: 594–603
12 Tang W, Hou YY, Wang XJ, *et al.* A hybrid of MnO_2 nanowires and MWCNTs as cathode of excellent rate capability for supercapacitors. J Power Sources, 2012, 197: 330–333
13 Rakhi RB, Chen W, Cha D, *et al.* Nanostructured ternary electrodes for energy storage applications. Adv Energy Mater, 2012, 2: 381–389
14 Peng L, Peng X, Liu B, *et al.* Ultrathin two-dimensional MnO_2/graphene hybrid nanostructures for high-performance, flexible planar supercapacitors. Nano Lett, 2013, 13: 2151–2157

15 Cheng Y, Zhang H, Lu S, *et al*. Flexible asymmetric supercapacitors with high energy and high power density in aqueous electrolytes. Nanoscale, 2013, 5: 1067–1073
16 Xu HH, Hu, XL, Sun YM, *et al*. Flexible fiber-shaped supercapacitors based on hierarchically nanostructured composite electrodes. Nano Res, 2015, 8: 1148–1158
17 Wang Z, Ma C, Wang H, *et al*. Facilely synthesized Fe_2O_3–graphene nanocomposite as novel electrode materials for supercapacitors with high performance. J Alloy Compd, 2013, 552: 486–491
18 Wang Z, Zhang X, Li Y, *et al*. Synthesis of graphene–$NiFe_2O_4$ nanocomposites and their electrochemical capacitive behavior. J Mater Chem A, 2013, 1: 6393–6399
19 Mahmood N, Tahir M, Mahmood A, *et al*. Role of anions on structure and pseudocapacitive performance of metal double hydroxides decorated with nitrogen-doped graphene. Sci China Mater, 2015, 58: 114–125
20 Dubal DP, Gund GS, Lokhande CD, *et al*. Decoration of spongelike $Ni(OH)_2$ nanoparticles onto MWCNTs using an easily manipulated chemical protocol for supercapacitors. ACS Appl Mater Interfaces, 2013, 5: 2446–2454
21 Wang Z, Zhang X, Wang JH, *et al*. Preparation and capacitance properties of graphene/NiAl layered double-hydroxide nanocomposite. J Colloid Interface Sci, 2013, 396: 251–257
22 Tu LL, Jia CY, Conducting polymers as electrode materials for supercapacitors. Prog Chem, 2010, 22: 1610–1618
23 Wang Y, Shi Z, Huang Y, *et al*. Supercapacitor devices based on graphene materials. J Phys Chem C, 2009, 113: 13103–13107
24 Williams GR, O'Hare D. Towards understanding, control and application of layered double hydroxide chemistry. J Mater Chem, 2006, 16: 3065–3074
25 Ma R, Liang J, Liu X, *et al*. General insights into structural evolution of layered double hydroxide: underlying aspects in topochemical transformation from brucite to layered double hydroxide. J Am Chem Soc, 2012, 134: 19915–19921
26 Shao M, Ning F, Zhao J, *et al*. Hierarchical layered double hydroxide microspheres with largely enhanced performance for ethanol electrooxidation. Adv Funct Mater, 2013, 23, 3513–3518
27 Shan D, Cosnier S, Mousty C. Layered double hydroxides: an attractive material for electrochemical biosensor design. Anal Chem, 2003, 75: 3872–3879
28 Chen H, Wang J M, Pan T, *et al*. Physicochemical properties and electrochemical performance of al-substituted α $Ni(OH)_2$ with additives for Ni-metal hydride batteries. J Electrochem Soc, 2003, 150: A1399–A1404
29 Wang Y, Zhang D, Peng W, *et al*. Electrocatalytic oxidation of methanol at Ni–Al layered double hydroxide film modified electrode in alkaline medium. Electrochim Acta, 2011, 56: 5754–5758
30 Niu Y, Li R, Li Z, *et al*. High-performance supercapacitors materials prepared via *in situ* growth of NiAl-layered double hydroxide nanoflakes on well-activated graphene nanosheets. Electrochim Acta, 2013, 94: 360–366
31 Li M, Zhu JE, Zhang L, *et al*. Facile synthesis of NiAl-layered double hydroxide/graphene hybrid with enhanced electrochemical properties for detection of dopamine. Nanoscale, 2011, 3: 4240–4246
32 Cheng Y, Zhang H, Varanasi CV, *et al*. Improving the performance of cobalt–nickel hydroxide-based self-supporting electrodes for supercapacitors using accumulative approaches. Energy Environ Sci, 2013, 6: 3314–3321
33 Yu C, Yang J, Zhao C, *et al*. Nanohybrids from NiCoAl-LDH coupled with carbon for pseudocapacitors: understanding the role of nano-structured carbon. Nanoscale, 2014, 6: 3097–3104
34 Srinivas G, Zhu Y, Piner R, *et al*. Synthesis of graphene-like nanosheets and their hydrogen adsorption capacity. Carbon, 2010, 48: 630–635
35 Wang L, Wang D, Dong X Y, *et al*. Layered assembly of graphene oxide and Co–Al layered double hydroxide nanosheets as electrode materials for supercapacitors. Chem Comm, 2011, 47: 3556–3558
36 Mulfinger L, Solomon SD, Bahadory M, *et al*. Synthesis and study of silver nanoparticles. J Chem Educ, 2007, 84: 322–325
37 Zhu Y, Cao C, Tao S, *et al*. Ultrathin nickel hydroxide and oxide nanosheets: synthesis, characterizations and excellent supercapacitor performances. Sci Rep, 2014, 4, 5787–5793
38 Xu J, Gai S, He F, *et al*. A sandwich-type three-dimensional layered double hydroxide nanosheet array/graphene composite: fabrication and high supercapacitor performance. J Mater Chem A, 2014, 2: 1022–1031
39 Lei Z, Lu L, Zhao XS. The electrocapacitive properties of graphene oxide reduced by urea. Energy Environ Sci, 2012, 5: 6391–6399
40 Gerbec JA, Magana D, Washington A, *et al*. Microwave-enhanced reaction rates for nanoparticle synthesis. J Am Chem Soc, 2005, 127: 15791–15800
41 Wu ZS, Ren W, Wang DW, *et al*. High-energy MnO_2 nanowire/graphene and graphene asymmetric electrochemical capacitors. ACS nano, 2010, 4: 5835–5842
42 Kong LB, Liu M, Lang JW, *et al*. Asymmetric supercapacitor based on loose-packed cobalt hydroxide nanoflake materials and activated carbon. J Electrochem Soc, 2009, 156: A1000–A1004
43 Wang H, Casalongue HS, Liang Y, *et al*. $Ni(OH)_2$ nanoplates grown on graphene as advanced electrochemical pseudocapacitor materials. J Am Chem Soc, 2010, 132: 7472–7477
44 Wang Z, Zhang X, Wang J, *et al*. Preparation and capacitance properties of graphene/NiAl layered double-hydroxide nanocomposite. J Colloid Interface Sci, 2013, 396: 251–257
45 Biswas S, Drzal LT, Biswas S, *et al*. Multilayered nanoarchitecture of graphene nanosheets and polypyrrole nanowires for high performance supercapacitor electrodes. Chem Mater, 2010, 22: 5667–5671
46 Zhang X, Shi W, Zhu J, *et al*. Synthesis of porous NiO nanocrystals with controllable surface area and their application as supercapacitor electrodes. Nano Res, 2010, 3: 643–652
47 Gupta BK, Thanikaivelan P, Narayanan TN, *et al*. Optical bifunctionality of europium-complexed luminescent graphene nanosheets. Nano Lett, 2011, 11: 5227–5233

Acknowledgment This work was supported by the National Natural Science Foundation of China (21573119, 21221062, 21131004, 21390393 and U1463202), and the Postdoctoral Science Foundation of China (2014M550710).

Author contributions Wang Z, Jia W, Chen C and Li Y designed the project and the experiments. Wang Z and Jiang M performed the experiments. Wang Z and Chen C analyzed the results and wrote the paper.

Conflict of interest The authors declare that they have no conflict of interest.

Zhuo Wang obtained her BSc degree from Liaoning Normal University and PhD degree from the Research Center for Eco-Environmental Sciences, Chinese Academy of Sciences. She was then a postdoctoral fellow at the Department of Chemistry, Tsinghua University. She is currently working at the Institute of Electrical Engineering of the Chinese Academy of Sciences (IEECAS), China. Her research concerns controlled synthesis of nanocomposites and nanomaterials for supercapacitors and batteries.

Chen Chen received his BSc degree from the Department of Chemistry, Beijing Institute of Technology in 2006, and PhD degree from the Department of Chemistry, Tsinghua University in 2011 under the direction of Prof. Yadong Li. After postdoctoral work at Lawrence Berkeley National Laboratory with Prof. Peidong Yang, he joined the Department of Chemistry at Tsinghua University as an associate professor in 2015. His research interests are focused on nanomaterials and catalysis.

中文摘要 本文通过微波加热法设计合成了水滑石-石墨烯复合材料, 并对该材料进行了表征. 研究发现, 通过微波法合成的水滑石-石墨烯复合材料具有超薄大片结构, 是一种“层-层”剥离的结构, 该结构有利于减少石墨烯的团聚, 形成大规模片状水滑石材料. 对材料的电容性能表征发现, 该材料具有优异的充放电性能及良好的电化学稳定性, 是一种有潜力的超级电容器电极材料.